THE JOURNAL OF BIOLOGICAL CHEMISTRY VOL. 286, NO. 15, pp. 13382–13392, April 15, 2011

Iron Mediates *N*-Methyl-D-aspartate Receptor-dependent Stimulation of Calcium-induced Pathways and Hippocampal Synaptic Plasticity*[S]

Received for publication, December 17, 2010, and in revised form, February 1, 2011 Published, JBC Papers in Press, February 4, 2011, DOI 10.1074/jbc.M110.213785

Pablo Muñoz[‡§1,2], Alexis Humeres[¶2], Claudio Elgueta[‡], Alfredo Kirkwood[‖], Cecilia Hidalgo[¶], and Marco T. Núñez[‡‡]**

*From the [‡]Centro de Neurociencia, Universidad de Valparaíso, Valparaíso 2360102, Chile, the [§]Centro Regional de Estudios en Alimentos Saludables, Valparaíso 2362696, Chile, [¶]Centro de Estudios Moleculares de la Célula, Facultad de Medicina, Universidad de Chile, Santiago 8380453, Chile, the [‖]Department of Neurosciences, The Johns Hopkins University, Baltimore, Maryland 21218, the **Programa de Fisiología y Biofísica, Instituto de Ciencias Biomédicas, Facultad de Medicina, Universidad de Chile, Santiago 8389100, and the [‡‡]Departamento de Biología, Facultad de Ciencias, and Institute for Cell Dynamics and Biotechnology, Universidad de Chile, Santiago 7800024, Chile*

Iron deficiency hinders hippocampus-dependent learning processes and impairs cognitive performance, but current knowledge on the molecular mechanisms underlying the unique role of iron in neuronal function is sparse. Here, we investigated the participation of iron on calcium signal generation and ERK1/2 stimulation induced by the glutamate agonist *N*-methyl-D-aspartate (NMDA), and the effects of iron addition/chelation on hippocampal basal synaptic transmission and long-term potentiation (LTP). Addition of NMDA to primary hippocampal cultures elicited persistent calcium signals that required functional NMDA receptors and were independent of calcium influx through L-type calcium channels or α-amino-3-hydroxy-5-methyl-4-isoxazolepropionic acid receptors; NMDA also promoted ERK1/2 phosphorylation and nuclear translocation. Iron chelation with desferrioxamine or inhibition of ryanodine receptor (RyR)-mediated calcium release with ryanodine reduced calcium signal duration and prevented NMDA-induced ERK1/2 activation. Iron addition to hippocampal neurons readily increased the intracellular labile iron pool and stimulated reactive oxygen species production; the antioxidant *N*-acetylcysteine or the hydroxyl radical trapper MCI-186 prevented these responses. Iron addition to primary hippocampal cultures kept in calcium-free medium elicited calcium signals and stimulated ERK1/2 phosphorylation; RyR inhibition abolished these effects. Iron chelation decreased basal synaptic transmission in hippocampal slices, inhibited iron-induced synaptic stimulation, and impaired sustained LTP in hippocampal CA1 neurons induced by strong stimulation. In contrast, iron addition facilitated sustained LTP induction after suboptimal tetanic stimulation. Together, these results suggest that hippocampal neurons require iron to generate RyR-mediated calcium signals after NMDA receptor stimulation, which in turn promotes ERK1/2 activation, an essential step of sustained LTP.

Iron deficiency during early life is associated with significantly lower cognitive and behavioral infant development (1–3), severe deterioration of hippocampal neuronal function (4–6), and poor memory and spatial learning capabilities (7–9). Current understanding of the relationship between neuronal function and brain iron status is sparse, and the molecular mechanisms underlying the essential role of iron in neuronal function remain mostly unidentified. Nonetheless, a role for iron in synaptic plasticity and the associated generation of postsynaptic Ca^{2+} signals has begun to emerge (10–12).

Neurons obtain iron via transferrin-dependent and -independent uptake pathways. The iron concentration in cerebrospinal fluid is sufficient to saturate the binding capacity of transferrin (13). This feature highlights the need for transferrin-independent iron uptake, which is likely to occur in neurons that express the iron transporter DMT1, such as hippocampal pyramidal and granule cells, cerebellar granule cells, pyramidal cells of the piriform cortex, *substantia nigra*, and the ventral portion of the anterior olfactory nucleus (14–16). The high DMT1 expression levels in these neurons suggest that DMT1-mediated iron uptake is necessary for their function.

Iron uptake into neurons stimulates the generation of reactive oxygen species (ROS)[3] and modifies the redox potential established by the intracellular levels of oxidized and reduced glutathione (17). Consequently, by modifying the cellular redox potential, iron is likely to modulate the balance between reduced and oxidized sulfhydryl groups in proteins. Iron, through the Haber-Weiss and Fenton reactions, is also a net generator of ROS, including the highly reactive hydroxyl radical (18, 19).

* This work was supported by Millennium Scientific Initiative Grant ICM-P05-001-F (to M. T. N.), Fondecyt-FONDAP Grant 15010006 (to C. H.), and Fondo Nacional de Desarrollo Científico y Tecnológico Grant FONDECYT 3080046 (to P. M.).

[S] The on-line version of this article (available at http://www.jbc.org) contains supplemental Figs. S1–S5.

[1] To whom correspondence should be addressed: Centro de Neurociencia, Universidad de Valparaíso, Valparaíso, Chile. Tel.: 56-32-2508186; Fax: 56-32-2508027; E-mail: pmunoz@cnv.cl.

[2] Both authors contributed equally to this work.

[3] The abbreviations used are: ROS, reactive oxygen species; NMDA, *N*-methyl-D-aspartate; RyR, ryanodine receptor; LTP, long-term potentiation; AMPA, α-amino-3-hydroxy-5-methyl-4-isoxazolepropionic acid; LIP, labile iron pool; Fe-NTA, $FeCl_3$-sodium nitrilotriacetate; DCDHF-DA, 2′,7′-dichlorodihydrofluorescein diacetate; DCF, 2′,7′-dichlorofluorescein; DFO, desferrioxamine; NAC, *N*-acetylcysteine; ACSF, artificial cerebrospinal fluid; TBS, theta burst stimulation; CREB, cAMP-response element-binding protein; fEPSP, field excitatory postsynaptic potential.

A link between ROS and normal neuronal function has been established; it is now known that activity-dependent hippocampal ROS generation is required for synaptic plasticity and memory (20). Glutamate or *N*-methyl-D-aspartate (NMDA) enhance ROS production (21, 22), and recent studies indicate that NMDA receptor activation enhances superoxide generation through NADPH oxidase stimulation (23, 24). Noteworthy, Fenton-generated hydroxyl radicals have a key role in NMDA-induced neuronal toxicity in cortical neurons in culture (25). Moreover, the redox-sensitive ryanodine receptor (RyR) Ca^{2+} release channels, which contribute to generate the postsynaptic Ca^{2+} signals required for sustained LTP (26, 27) are likely targets for iron-generated ROS. In fact, iron promotes RyR-mediated Ca^{2+} release in PC12 cells (28).

Here, we used cultured hippocampal neurons to study the effects of iron addition or iron chelation on NMDA receptor-dependent Ca^{2+} signal generation and ERK1/2 activation. We also investigated in hippocampal slices the effects of iron addition/chelation on basal synaptic transmission and LTP. Our results indicate that iron is essential to elicit RyR-mediated Ca^{2+} signals following NMDA receptor stimulation, and that these Ca^{2+} signals stimulate ERK1/2 phosphorylation, a requisite step of sustained hippocampal CA1 LTP. Our results also show that iron is required for basal synaptic transmission and sustained hippocampal LTP.

EXPERIMENTAL PROCEDURES

Antibodies—Monoclonal phospho-ERK1/2 and polyclonal ERK1/2 antibodies were obtained from Santa Cruz Biotechnology. Monoclonal anti-β-actin antibody was from Sigma. Alexa Fluor 594-conjugated goat anti-mouse and Alexa Fluor 488-conjugated goat anti-rabbit antibodies were obtained from Invitrogen.

Primary Hippocampal Cultures—The hippocampus from Sprague-Dawley rats was dissected at embryonic day 18, and primary cultures were prepared using standard procedures (29). Cells were initially plated in minimal essential medium, 10% horse serum and maintained in an incubator at 37 °C under 5% CO_2. Three h after plating, the minimal essential medium was replaced by serum-free Neurobasal medium supplemented with B27 and 2 mM Glutamax™ (Invitrogen). Medium was changed every 72 h. Cells were used 11–14 days after plating.

Ca^{2+} Imaging—To record Ca^{2+} signals elicited by NMDA (Calbiochem), hippocampal cells grown in coverslips for 11 to 14 days were incubated at 37 °C with 5 μM Fluo-3-AM (Molecular Probes) in Neurobasal medium. After 30 min of incubation to allow dye entry and de-esterification, coverslips were washed 3 times with Mg^{+2}-free Hanks' buffered salt solution, containing (in mM) 118 NaCl, 4.8 KCl, 3 $CaCl_2$, 10 glucose, 20 Hepes/Tris, pH 7.4, plus 10 μM glycine (recording solution). After this washing period, which lasted 15 min, cells were transferred to a Maximov assembly chamber, bathed in a 1-ml recording solution and immediately tested. Cell-associated fluorescence (excitation 488 nm; emission 505–530 nm) was determined in a Zeiss LSM 510 Meta laser confocal scanning microscope. After NMDA addition, fluorescence was monitored continuously by taking frames at 10–30-s intervals using the microscope single-track mode. To inhibit NMDA receptor function, cultures were preincubated for 1 h with 50 μM MK-801 (Calbiochem). In some cases, cultures were preincubated for 10 min prior to NMDA addition with 10 μM 6-cyano-7-nitroquinoxaline-2,3-dione (Sigma) to inhibit α-amino-3-hydroxy-5-methyl-4-isoxazolepropionic acid (AMPA) receptors, plus 10 μM nifedipine (RBI) to inhibit voltage-gated L-type Ca^{2+} channels. Other cultures were preincubated for 20 min with 1 μM tetrodotoxin before addition of NMDA. To investigate the effects of depolarization on Ca^{2+} signal generation, cultures were incubated for 5 min with extracellular solutions containing 80 mM KCl; to maintain osmolarity the NaCl concentration was decreased accordingly.

To test the effects of iron addition on Ca^{2+} signal generation, hippocampal cells loaded with Fluo-3 AM as above were transferred 15 min prior to recording to Ca^{2+}-free Hanks' buffered salt solution, containing (in mM) 119.6 NaCl, 4.7 KCl, 4.2 $MgCl_2$, 10 glucose, 20 Hepes/Tris, pH 7.4, plus 0.5 EGTA/Tris.

Fluo-3 fluorescence values are presented as F/F_o, where F is the fluorescence recorded following NMDA or iron addition and F_o the mean basal fluorescence. All imaging experiments were done at room temperature.

Immunocytochemistry—Hippocampal cells were washed with PBS, fixed for 20 min in PBS containing 4% paraformaldehyde and 4% sucrose, and permeabilized for 10 min with 0.1% Triton X-100 in PBS. Cells were stained for phosphorylated ERK1/2 using anti-phospho-ERK1/2 monoclonal antibodies (dilution 1:50) and total ERK1/2 with anti-ERK rabbit polyclonal antibodies (dilution 1:200). Following incubation, cells were washed and incubated with a mixture of Alexa Fluor 594-conjugated goat anti-mouse antibody (1:200) together with Alexa Fluor 488-conjugated goat anti-rabbit antibody (1:200). Fixed cells were imaged with a Zeiss LSM 510 laser scanning fluorescence microscope. High magnification fields from each culture condition were imaged with an Axiocam HR camera attached to a PC equipped with Axiovision software, using a multitrack configuration with two different excitation wavelengths (excitation 543 nm, filter 560 nm for Alexa Fluor 488, and excitation 488 nm, filter 505–530 nm for Alexa Fluor 594). Nuclei were detected by confocal microscopy (excitation at 350 nm with a fluorescent lamp; emission 460 nm) following incubation of cultures for 10 min with 2 μg/ml of Hoechst stain (Invitrogen).

Western Blot Analysis—Cells extracts were prepared as described (30). Proteins were resolved in 10% Laemmli SDS-polyacrylamide gels, transferred to polyvinylidene fluoride membranes (Millipore Corp.), and incubated overnight with primary antibody. Dilutions for primary antibodies were 1:500 for phospho-ERK1/2 and 1:10,000 for total ERK1/2. To correct for loading, membranes were stripped and re-probed with monoclonal anti-β-actin antibody. The Image J image processing and analysis program (National Institutes of Health, Bethesda, MD) was used to quantify optical band density.

Determination of the Labile Iron Pool—The cellular labile iron pool (LIP) was determined with the fluorescence probe calcein as described (31, 32). In brief, cultured hippocampal cells were incubated for 30 min with 0.5 μM calcein-AM and calcein fluorescence was determined as a function of time by confocal microscopy. After baseline fluorescence collection,

the medium was supplemented with Fe^{3+} as the complex $FeCl_3$-sodium nitrilotriacetate (Fe-NTA, 1:2.2, mol:mol) (17). Images were acquired at a sampling rate of 50 ms/line and 0.07 μm/pixel using the microscope in the line-scan mode, with radial and axial resolutions of 0.4 and 1.0 μm, respectively. The decrease in calcein fluorescence was taken as an indication of increased LIP. Calcein signals are presented as F/F_o values, defined as described above.

Iron-induced ROS Generation—Iron-induced ROS generation was determined using 2′,7′-dichlorodihydrofluorescein diacetate (DCDHF-DA; Invitrogen), a ROS-sensitive membrane-permeable fluorescent probe, as described (17). DCDHF-DA is hydrolyzed inside cells to the non-fluorescent compound DCDHF, which emits fluorescence when oxidized to 2′,7′-dichlorofluorescein (DCF). Thus, the fluorescence emitted by DCF directly reflects the overall oxidative status of a cell. DCF fluorescence (excitation: 488 nm; emission 500–560 nm) was recorded before and after the addition of 50 μM ferrous ammonium sulfate. The endogenous iron content was previously lowered by preincubation overnight in complete medium to which 3 μM desferrioxamine (DFO; Sigma) was added. After DFO removal, cells were loaded for 30 min with 5 μM DCDHF-DA in Neurobasal medium as described (17). In some experiments, the effects on ROS formation of preincubation for 1 h with 50 μM MCI-186 (Santa Cruz Biotechnology), an hydroxyl radical and nitric oxide scavenger (33, 34), or for 4 h with 0.1 mM *N*-acetylcysteine (NAC), a general antioxidant, were tested.

Electrophysiology—Hippocampal slices (400 μm) were prepared from 3- to 5-week-old Long-Evans rats in ice-cold dissection buffer (in mM: 212.7 sucrose, 2.6 KCl, 1.23 NaH_2PO_4, 26 $NaHCO_3$, 3 $MgCl_2$, 1 $CaCl_2$, and 10 dextrose, bubbled with a mixture of 5% CO_2 and 95% O_2). Slices were incubated for 1 h at room temperature in artificial cerebrospinal fluid (ACSF, in mM: 124 NaCl, 5 KCl, 1.25 NaH_2PO_4, 26 $NaHCO_3$, 1.5 $MgCl_2$, 2.5 $CaCl_2$, and 10 dextrose, bubbled with a mixture of 5% CO_2 and 95% O_2). Unless otherwise specified, all recordings were done in a submersion-recording chamber perfused with ACSF (30 ± 0.5 °C; 2 ml/min). Synaptic responses, evoked by stimulating the Schaffer collaterals with 0.2-ms pulses delivered through concentric bipolar stimulating electrodes, were recorded with extracellular electrodes placed in CA1 *stratum radiatum*. Baseline responses were recorded using half-maximum stimulation intensity at 0.033 Hz. Paired-pulse stimulation (40-ms inter stimulus interval) was used throughout the experiment unless stated otherwise. LTP was induced by theta burst stimulation (TBS), consisting of four θ epochs delivered at 0.1 Hz. Each epoch, in turn, consisted of 10 trains of four pulses (at 100 Hz) delivered at 5 Hz. Only data from slices with stable recordings (<5% change over the baseline period) were included in the analysis. All data are presented as mean ± S.E. normalized to the pre-conditioning baseline.

To record miniature excitatory spontaneous postsynaptic currents, hippocampal slices held at the bottom of the perfusion chamber were observed under an upright microscope equipped with infrared differential interference contrast (BX51WI, Olympus). Whole cell recordings of CA1 pyramidal cells were obtained using glass electrodes with a resistance of 2–5 MΩ, filled with a solution containing (mM) 135 K-gluconate, 5 KCl, 4 Na_2ATP, 0.4 Na_2GTP, 5 EGTA, 10 Hepes/Tris, pH 7.4. Signals were amplified and low-pass filtered (1 kHz) using an EPC-7 plus amplifier (HEKA electronic, Lambretch, Germany), digitized at 20 kHz (PCI-6221, National Instruments, Austin, TX) and acquired using custom routines written in IGOR PRO (Wavemetrics). Series resistance, calculated online by measuring the peak of an unfiltered current evoked by a 10-mV step, was always below 15 MΩ and was left uncompensated. Miniature excitatory spontaneous postsynaptic currents were recorded in normal oxygenated ACSF at 32 °C, supplemented with 1 μM tetrodotoxin. Analysis was performed using MiniAnalysis Software (Synaptosoft Inc.).

Statistical Analysis—One-way analysis of variance was used to test for differences in mean values from multiple samples, and Dunnett's or Newman-Keuls post-hoc test were used for comparisons (InStat program from GraphPad). Statistical differences between two means were analyzed by two-tailed unpaired Student's *t* test. Differences were considered significant if $p < 0.05$.

RESULTS

Persistent NMDA-induced Ca^{2+} Signals in Cultured Hippocampal Neurons Require Iron and RyR-mediated Ca^{2+} Release—Early studies indicate that NMDA receptor activation by tetanic stimulation generates RyR-dependent Ca^{2+} signals in hippocampal slices (35). We investigated here the effects of decreasing iron and the contribution of RyR-mediated Ca^{2+} release to Ca^{2+} signals elicited by NMDA in primary hippocampal neurons. To test the effects of iron removal, we preincubated primary cultures with DFO, a highly selective siderophore produced by aerobic bacteria to ensure Fe^{3+} acquisition under conditions of iron starvation (36–39). DFO displays high affinity for iron and is a weak Ca^{2+} chelator; log stability constants of 30.6 and 2.6 have been reported for Fe^{3+} and Ca^{2+}, respectively (38). To suppress RyR-mediated Ca^{2+} release, we preincubated cultures for 1 h with 50 μM ryanodine, a highly selective RyR inhibitor that in these conditions abolishes RyR-mediated Ca^{2+} release in primary hippocampal neurons (29).

Processes of hippocampal neurons that displayed postsynaptic markers (Fig. 1*A*), exhibited long-lasting increases in Fluo-3 fluorescence after addition of 50 μM NMDA (washed after 5 min of incubation); this fluorescence increase was detectable 20 and 30 min after NMDA addition (Fig. 1, *B*, *top panel*, and *C*). In contrast, neurons preincubated for 1 h with 500 μM DFO or 50 μM ryanodine before NMDA addition displayed increased fluorescence at 10 min but not at 20 or 30 min after addition of NMDA (Fig. 1, *B*, *middle* and *lower panels*, and *C*).

Addition of NMDA to neurons preincubated with DFO elicited an initial fluorescence increase of lower magnitude than that observed in controls, which immediately started to decay to basal levels after NMDA removal (Fig. 1*C*). Neurons preincubated with ryanodine displayed after NMDA addition an initial fluorescence increase of similar magnitude as controls, which also started to decay to basal levels immediately after NMDA removal (Fig. 1*C*). These combined observations strongly suggest that the initial Ca^{2+} increase produced by 50 μM NMDA represents mainly Ca^{2+} entry caused by NMDA

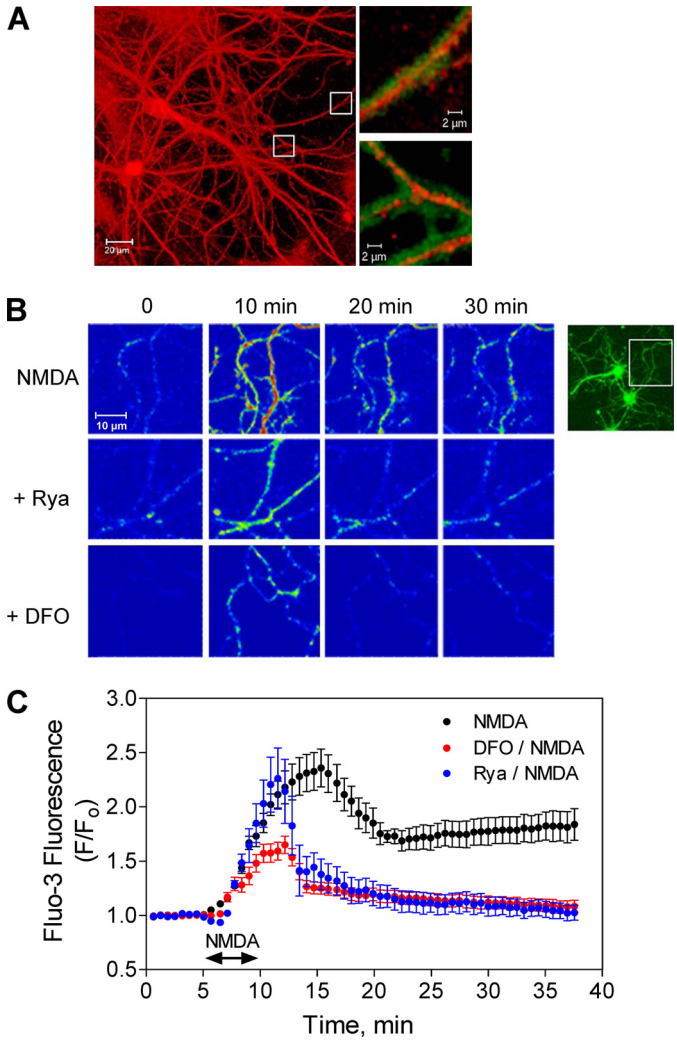

FIGURE 1. **NMDA-induced Ca^{2+} signals in cultured hippocampal neurons: inhibitory effects of DFO and ryanodine.** *A*, cultured hippocampal neurons were sequentially labeled with antibodies against the neuronal marker MAP1-B (*red*) and the synapse marker PSD-95 (*green*). *Insets* show double-labeled synaptic regions. *B*, hippocampal neurons were preincubated for 1 h with culture medium, or with medium containing 50 μM ryanodine (*Rya*) or 500 μM DFO. After washing out these reagents, cells were loaded with Fluo-3-AM and exposed for 5 min to a solution containing 50 μM NMDA. Shown are sequential confocal images of neuronal processes, taken at the indicated time intervals after NMDA addition. *C*, Fluo-3 fluorescence intensity values, obtained from recordings described in *B*, were normalized against the fluorescence values obtained before NMDA addition (F/F_o) and plotted as a function of time. Data represent mean ± S.E. ($n = 3$).

receptor stimulation, whereas the long-lasting component that persists after NMDA removal arises from RyR-mediated Ca^{2+}-induced Ca^{2+} release, because when RyR channels were inhibited with ryanodine the signals rapidly returned to basal levels following NMDA removal (Fig. 1, *B* and *C*). Iron seems to participate in the generation of the early component, because iron chelation with DFO reduced the initial Ca^{2+} signal produced by NMDA. Iron is also required for the delayed component, presumably to set the oxidative tone required for RyR-mediated Ca^{2+}-induced Ca^{2+} release, because prolongation of the Ca^{2+} signal after NMDA removal was prevented by iron chelation with DFO.

Preincubation with the NMDA receptor inhibitor MK-801 (50 μM, 60 min) before addition of NMDA completely suppressed the fluorescence increase caused by NMDA (supplemental Fig. S1*A*). In contrast, NMDA-generated Ca^{2+} signals were not affected by joint preincubation with 10 μM nifedipine to inhibit L-type Ca^{2+} channels plus 10 μM 6-cyano-7-nitroquinoxaline-2,3-dione to inhibit AMPA receptors (supplemental Fig. S1*B*). Selective Na^+ channel block with tetrodotoxin did not affect the Ca^{2+} signals induced by addition of NMDA for 5 min (supplemental Fig. S1*C*), showing that these signals did not arise from NMDA-induced massive neuronal depolarization. Moreover, addition of 80 mM KCl for 5 min produced only a transient increase in intracellular Ca^{2+} that decayed rapidly to basal levels 5 min after KCl removal (supplemental Fig. S1*D*). These results indicate that NMDA-triggered Ca^{2+} influx via NMDA receptors produces Ca^{2+} signals that lack significant contributions from other potential Ca^{2+} entry pathways.

Iron and RyR-mediated Ca^{2+} Release Are Required for NMDA-induced ERK1/2 Phosphorylation and Nuclear Translocation—NMDA binding to its receptor activates the Ca^{2+}-responsive ERK1/2 pathway (40–42). In agreement with these reports, we found that hippocampal slices from adult rats incubated for 5 min with 50 μM NMDA displayed a small but significant enhancement of ERK1/2 phosphorylation when measured 60 min after stimulation for 5 min with NMDA. This enhancement was inhibited by preincubation of slices for 1 h with 500 μM DFO or 50 μM ryanodine (Fig. 2, *A* and *B*), suggesting that ERK1/2 activation requires both iron and the persistent postsynaptic Ca^{2+} signals generated by RyR-mediated Ca^{2+} release.

Translocation of the phosphorylated ERK1/2 proteins to the nucleus, where they promote the downstream phosphorylation of the transcription factor cAMP-response element-binding protein (CREB), is a crucial step for the induction of some forms of long-lasting potentiation (43). Our immunofluorescence studies revealed that primary hippocampal neurons exhibit low levels of phosphorylated ERK1/2 proteins with a predominant cytoplasmic localization (Fig. 2*C*, *first row of panels*); preincubation for 1 h with 50 μM ryanodine or 500 μM DFO did not modify these basal levels (Fig. 2*C*, *second* and *third row of panels*). Incubation with 50 μM NMDA for 5 min promoted ERK1/2 phosphorylation and nuclear translocation (Fig. 2*C*, *fourth row of panels*). Preincubation for 1 h with 50 μM ryanodine or 500 μM DFO prior to NMDA addition significantly inhibited the nuclear translocation of the phosphorylated ERK1/2 proteins induced by NMDA (Fig. 2*C*, *fifth* and *sixth row panels*). The average results shown in Fig. 2*D* confirm that preincubation of hippocampal neurons with DFO or ryanodine decreased by 75% the enhanced translocation of the phosphorylated ERK proteins induced by NMDA. The fact that this inhibition was not complete suggests that other pathways insensitive to DFO and ryanodine make a minor contribution to NMDA-induced ERK1/2 phosphorylation and nuclear translocation. The combined results illustrated in Fig. 2 suggest that the Ca^{2+}-dependent signaling cascades that link NMDA receptor stimulation to ERK1/2 activation in primary hippocampal neurons require functional RyR and iron for maximum activation.

Addition of Iron Increases Both the Cellular LIP and ROS—Addition of iron to the extracellular solution promotes iron uptake into hippocampal neurons in culture (44). A substantial

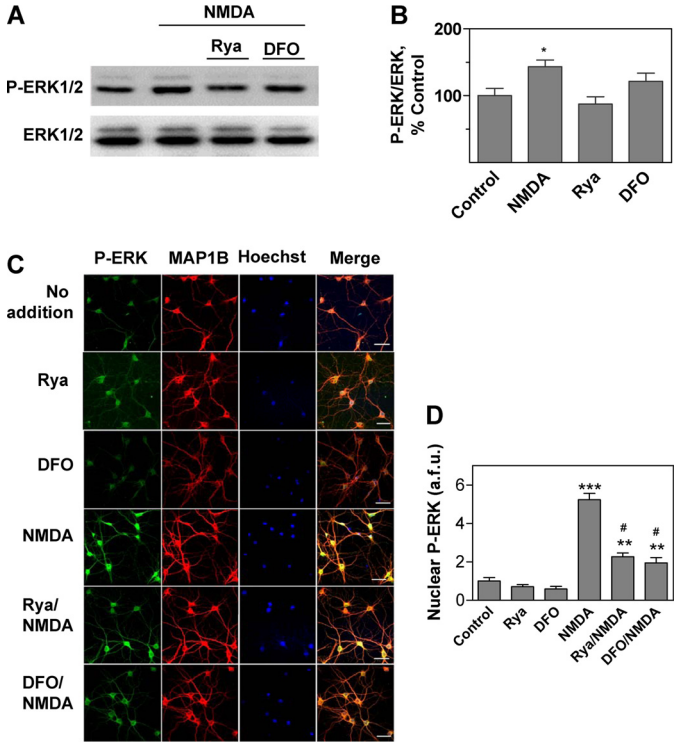

FIGURE 2. **ERK1/2 activation by NMDA in hippocampal slices and cultured hippocampal neurons: inhibitory effects of ryanodine and DFO.** *A*, hippocampal slices were exposed to a solution containing 50 μM NMDA for 5 min. When indicated, slices were preincubated for 1 h with 50 μM ryanodine or 500 μM DFO before addition of NMDA. Sixty min after NMDA addition, the CA1 area was dissected, homogenized, and extracts were analyzed by Western blotting. For blotting, proteins were first probed with an antibody that recognizes phosphorylated ERK1/2 (*upper panel*). Membranes were then stripped and re-probed with a total ERK1/2 antibody (*lower panel*). *B*, quantification of the Western blot band density of phosphorylated ERK1/2 (*P-ERK1/2*) referenced to the corresponding total ERK density. Values represent percentage of control and are given as mean ± S.E. ($n = 3$). *, $p < 0.05$. *C*, immunofluorescence images of cultured hippocampal neurons probed with phospho-ERK antibody (*green*, *left panels*) followed by an antibody against the neuronal marker MAP1-B (*red*); nuclei were stained with Hoechst (*blue*). The merged images are shown at the *right*. Neurons were incubated for 5 min with 50 μM NMDA and fixed 15 min after NMDA removal. Controls were mock-incubated without NMDA (*No addition*). When noted, neurons were preincubated for 1 h with 50 μM ryanodine (*Rya*) or 500 μM DFO, which when NMDA was added were removed before NMDA addition. *Bar*, 50 μm. *D*, nuclear localization of phospho-ERK1/2. Nuclear translocation of phosphorylated ERK1/2, expressed in arbitrary fluorescence units (*a.f.u.*), was determined by measuring phosphorylated ERK1/2 green fluorescence in the area defined by the Hoechst stain. The number of neurons considered in each case was: no addition, 23; NMDA, 28; DFO, 20; Rya, 18; Rya/NMDA, 18; DFO/NMDA, 21. Cells were from three independent cultures. Data represent mean ± S.E.; *, $p < 0.05$; **, $p < 0.01$; ***, $p < 0.001$ compared with control. #, $p < 0.001$ relative to cultures incubated only with NMDA.

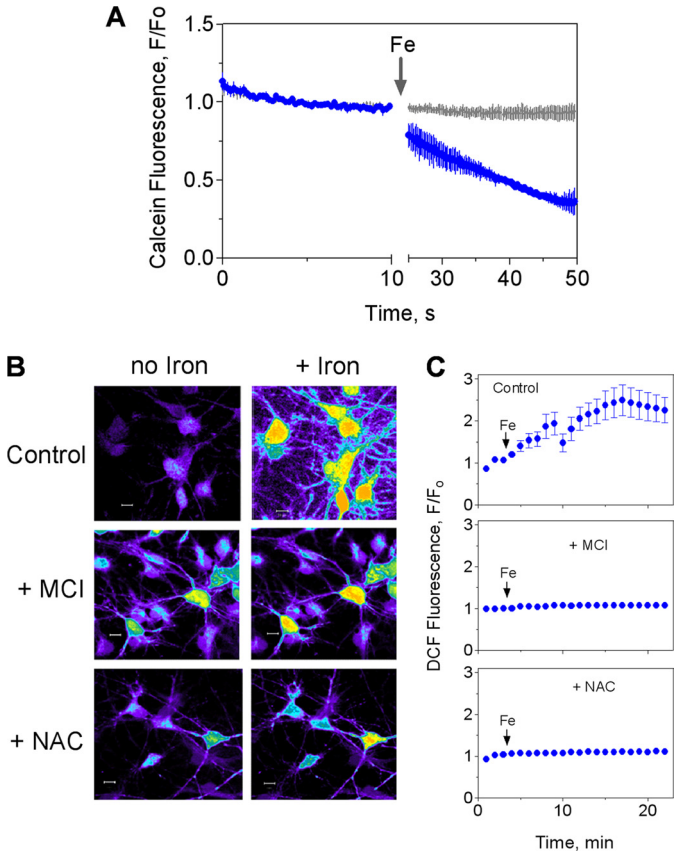

FIGURE 3. **Extracellular iron enters the cytoplasmic LIP and generates ROS.** *A*, iron entry into the LIP. Fluorescence record as a function of time of primary hippocampal neurons loaded with the iron sensor calcein before and after addition of 100 μM Fe-NTA (*blue trace*). Calcein fluorescence was also measured in control cells (*gray trace*) ($n = 5$). *B*, iron-induced ROS production. Cultured hippocampal neurons were preincubated overnight with 3 μM DFO to lower their endogenous iron content. After washing out DFO, cells were loaded with the cell permeant redox sensor DCDHF-DA. When indicated, cells were preincubated for 1 h with 50 μM MCI-186 or 4 h with 100 μM NAC. These reagents were washed-off prior to DCDHF-DA loading. Fluorescence was recorded before (*left panels*) or 20 min after iron addition (*right panels*). *C*, panels illustrate the time course of average fluorescence changes in control conditions following iron addition (*arrows*) or in cells preincubated with MCI-186 or NAC as in *B*. Images were taken from cell processes. Data represent mean ± S.E. ($n = 4$).

fraction of the iron taken up by cells joins the LIP, where iron engages in redox reactions (45, 46) leading to an increase of cellular ROS. This iron-induced ROS increase is likely to promote Ca^{2+} release through the highly redox-sensitive RyR channels (47–49), providing the strong Ca^{2+} signals required for stimulating the ERK1/2 cascade. We previously reported that iron addition elicits RyR-mediated Ca^{2+} signals and stimulates the ERK1/2 cascade in PC12 cells (28). Accordingly, we tested here if in primary hippocampal neurons addition of iron promotes ROS generation, RyR-mediated Ca^{2+} release, and ERK1/2 activation.

We found that iron addition resulted in a significant increase of the LIP, as detected by calcein quenching (Fig. 3*A*). To investigate if iron addition also stimulated ROS generation, we measured intracellular ROS levels with the ROS-sensitive probe DCDHF-DA. Both neurons and glial cells displayed significant ROS generation following addition of iron, as demonstrated by an increase in DCF fluorescence relative to the control (Fig. 3*B*, *top panels*). Fluorescence intensity records taken from cell processes indicated that DCF fluorescence was stabilized 15 min after iron addition (Fig. 3*C*, *top panel*). Preincubation for 1 h with the hydroxyl radical scavenger MCI-186 (45, 50) markedly decreased iron-mediated ROS generation (Fig. 3*B*, *middle panel*); this reduction was especially noticeable in cell processes (Fig. 3*C*, *middle panel*). Similarly, a 4-h preincubation with the antioxidant NAC significantly decreased the iron-induced ROS increase (Fig. 3, *B* and *C*, *lower panels*). Taken together, these results indicate that addition of iron to hippocampal neurons in culture increased the labile iron pool and caused an increase in cellular ROS, including Fenton-derived hydroxyl radicals.

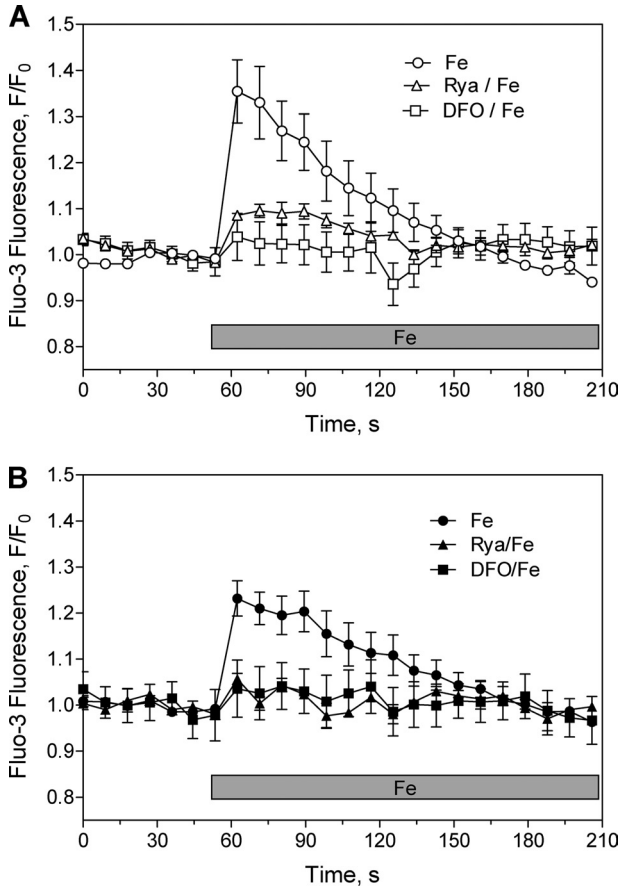

FIGURE 4. **Iron produces RyR-mediated Ca^{2+} signals.** Cultured hippocampal neurons were loaded with the fluorescent Ca^{2+} sensor Fluo-3 AM and transferred to Ca^{2+}-free solution; changes in probe fluorescence were detected after addition of 20 μM Fe-NTA as described under "Experimental Procedures." The fluorescence changes were detected in cell soma (*top*) or cell processes (*bottom*). When noted, cells were preincubated for 1 h with 50 μM ryanodine or 500 μM DFO before iron addition, and iron was added after removal of these reagents. Data represent mean ± S.E. from three independent experiments.

Iron Stimulation of RyR-mediated Ca^{2+} Release and ERK1/2 Phosphorylation in Hippocampal Neurons—To examine if iron participates in Ca^{2+} signal generation, as suggested by the inhibitory effects of DFO on NMDA-dependent Ca^{2+} increase and ERK phosphorylation, we loaded cultured hippocampal neurons with the Ca^{2+}-sensitive probe Fluo-3 AM, and determined changes in fluorescence by confocal image detection. Addition of 20 μM iron to neurons maintained in Ca^{2+}-free solution caused a significant increase in the Fluo-3 fluorescence of individual neurons (supplemental Fig. S2). Average values obtained from fluorescence records taken from cell soma (Fig. 4*A*) or neuronal processes (Fig. 4*B*) show that this Ca^{2+} increase was transitory and returned to basal levels within 1 min after iron addition. The Ca^{2+} increase induced by iron required functional RyR, because it did not occur in cultures preincubated with ryanodine; DFO also prevented this increase, showing that DFO is an effective iron chelator in the conditions used in these experiments (Fig. 4, *top* and *bottom panels*).

We have previously shown that ERK1/2 phosphorylation increases significantly following iron addition to PC12 cells kept in Ca^{2+}-free solution (28). Concurring with that report, incubation of hippocampal slices with iron for 1 h produced a significant enhancement of ERK1/2 phosphorylation in the CA1 region, which was prevented by preincubation of slices with 50 μM ryanodine or 500 μM DFO (Fig. 5, *A* and *B*). Incubation of hippocampal neurons with iron for 60 min induced nuclear translocation of phosphorylated ERK1/2, as determined by immunocytochemistry (Fig. 5, *C* and *D*). Nuclear translocation of phosphorylated ERK1/2 did not occur in cells previously incubated with either ryanodine or DFO (Fig. 5, *C* and *D*). It is important to point out that, in contrast to the stimulation of ERK1/2 phosphorylation induced by NMDA, which was significantly but not completely inhibited by DFO and ryanodine, these two compounds completely suppressed iron-induced ERK1/2 phosphorylation. In addition, we confirmed that exposure of hippocampal slices to H_2O_2 (200 μM), followed by CA1 area dissection and Western blot analysis of ERK1/2 proteins, significantly enhanced ERK1/2 phosphorylation in the CA1 region (supplemental Fig. S3), as previously reported (29). This stimulation was abolished by preincubation of slices for 1 h with 50 μM ryanodine prior to H_2O_2 addition. Moreover, a 1-h preincubation with 500 μM DFO also prevented H_2O_2-induced ERK1/2 phosphorylation (supplemental Fig. S3). These results show that both iron and RyR-mediated Ca^{2+} release contribute to stimulate ERK1/2 phosphorylation in response to exogenous H_2O_2 addition. The combined results shown in Figs. 3–5 strongly suggest that iron-generated ROS via activation of RyR-mediated Ca^{2+} release produce an intracellular [Ca^{2+}] increase that stimulates ERK1/2 phosphorylation and translocation to the nucleus.

Iron, Synaptic Transmission, and LTP—The above findings suggest that iron chelation prevents the emergence of the RyR-mediated Ca^{2+} signals induced by NMDA receptor activation that promotes ERK1/2 phosphorylation, a requisite step of sustained synaptic plasticity. Therefore, we tested if iron chelation with DFO affected basal synaptic transmission, LTP induction, and LTP maintenance.

To measure basal synaptic transmission, field excitatory postsynaptic potentials (fEPSP) were registered in slices stimulated with paired pulses separated by 40 ms. As illustrated in Fig. 6*A*, addition of DFO to hippocampal slices produced a significant decrease in the postsynaptic response ($p < 0.001$); basal synaptic transmission recovered partially after DFO removal but persisted at levels lower than controls even for 40 min after DFO removal. Noteworthy, slices that were not stimulated during the incubation with DFO displayed normal basal synaptic transmission when stimulated after DFO removal (Fig. 6*A*, *solid symbols*), indicating that DFO-induced depression is activity-dependent. Consistent with that, application of DFO alone did not affect the amplitude and frequency of miniature spontaneous excitatory postsynaptic currents (supplemental Fig. S4). Most probably, DFO depressed the postsynaptic response, because DFO did not affect paired-pulse facilitation, a presynaptic property (Fig. 6*B*). Interestingly, preincubation with DL-2-amino-5-phosphonopentanoic acid, a specific antagonist of NMDA receptors, prevented the synaptic depression caused by DFO (Fig. 6*C*), indicating that the DFO-induced depression requires functional NMDA receptors.

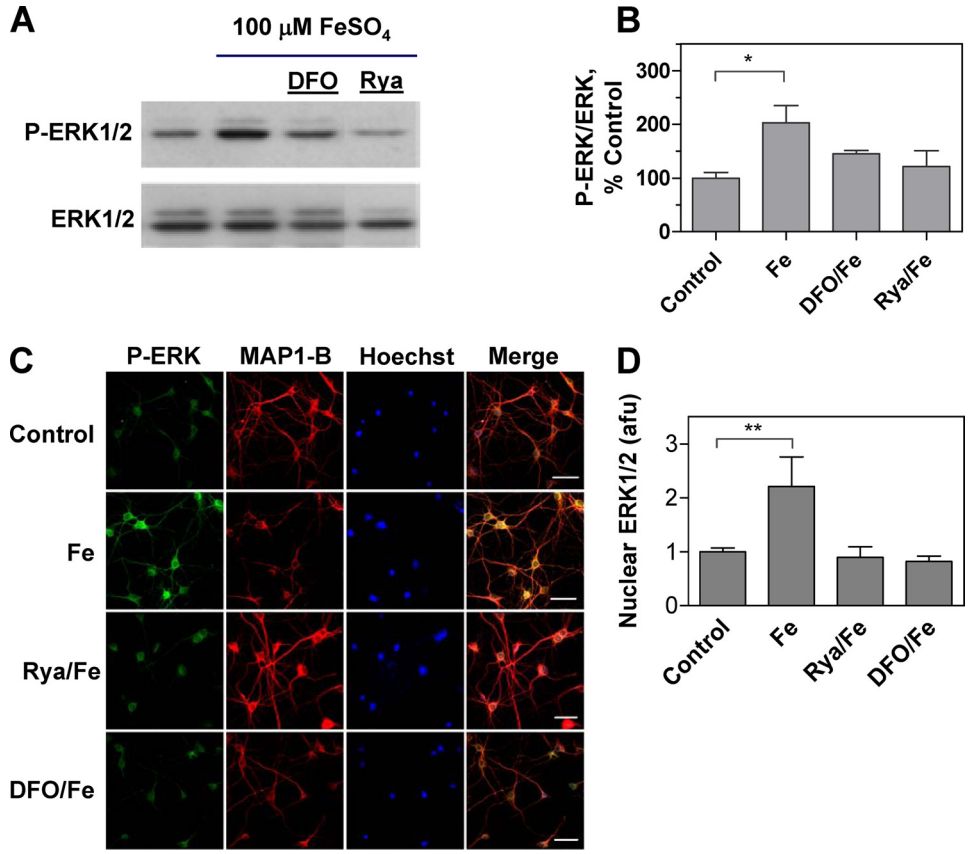

FIGURE 5. **Iron activates ERK1/2 phosphorylation and nuclear translocation.** *A*, ERK1/2 phosphorylation was analyzed by Western blots of the hippocampal CA1 area, which was dissected from control slices or from slices exposed for 1 h to 100 μM $FeSO_4$. When noted, neurons were preincubated for 1 h with 50 μM ryanodine or 500 μM DFO. These reagents were removed before iron addition. *B*, quantification of phospho-ERK1/2 immunoreactivity normalized to total ERK1/2 for data such as shown in *A*; data represent mean ± S.E. from three independent experiments. *, $p < 0.05$, compared with the control. *C*, iron-induced nuclear translocation of phospho-ERK1/2. Cultured hippocampal neurons were stained with an antibody against phosphorylated ERK1/2 (*green*, *left panels*) followed by an antibody against the neuronal marker MAP1-B (*red*). Nuclei were stained with Hoechst (*blue*). The merged images are shown in the *right panels*. Immunostaining was performed before (*Control*) or 1 h after addition of 20 μM Fe-NTA (*Fe*). When noted, neurons were preincubated for 1 h with 50 μM ryanodine or 500 μM DFO before iron addition, as described in *A*. *D*, nuclear translocation of phosphorylated ERK1/2, expressed in arbitrary fluorescence units (*a.f.u.*), was determined by measuring phosphorylated ERK1/2 (green fluorescence) in the area demarcated by the Hoechst stain. Data represent mean ± S.E. from three independent experiments. **, $p < 0.01$ compared with the control.

In contrast to the effects of iron chelation, addition of 100 μM $FeSO_4$ produced a significant increase in the magnitude of the synaptic response (163.3 ± 2.1% of baseline at 60 min; $p < 0.05$), as illustrated in Fig. 7*A*, but did not affect paired pulse facilitation (supplemental Fig. S5*A*). This response was significantly inhibited ($p < 0.0001$) in slices preincubated with DFO for 1 h, followed by DFO removal before iron addition (Fig. 7*A*). The stimulatory effects of $FeSO_4$ were caused by iron and not by sulfate, because addition of 100 μM Na_2SO_4 induced a small decrease in fEPSP slope (supplemental Fig. S5*B*). Moreover, addition of iron in the form of Fe-NTA also produced an increase in the fEPSP slope, as observed with $FeSO_4$, although of smaller magnitude (supplemental Fig. S5*C*). Iron chelation by NTA decreases free iron availability; this may explain why Fe-NTA elicited a smaller response than $FeSO_4$.

The above results strongly suggest that iron by itself promotes synaptic activity. Therefore, we tested next whether moderate levels of iron facilitate the induction of LTP with suboptimal tetanic stimulation. As shown in Fig. 7*B*, conditioning stimulation with one TBS epoch resulted in transient potentiation of the response that returned to baseline within 60 min (95.0 ± 6.3% of baseline at 60 min). In contrast, in the presence of 20 μM iron, a concentration that did not affect baseline responses, one TBS epoch induced significant LTP (119.2 ± 5.8% of baseline at 60 min, $p < 0.005$).

We also investigated if iron chelation, produced by preincubating slices with DFO (1 mM, 20 min) in the absence of stimulation, impaired subsequent LTP induction with optimal tetanic stimulation. As shown in Fig. 7*C*, conditioning with 4 TBS epochs induced robust LTP in control slices but did not induce persistent changes in slices pretreated with DFO (control, 143.6 ± 12.1%; DFO, 100.9 ± 6.5%; two-tailed p value = 0.0009). Altogether, the results presented in this work strongly suggest that hippocampal neurons require iron to generate NMDA-induced and RyR-mediated Ca^{2+} signals that stimulate ERK1/2 phosphorylation, as well as for basal synaptic transmission and sustained LTP.

DISCUSSION

Limited but compelling evidence indicates that iron is necessary for hippocampus-dependent learning processes (4, 7–11). Until now, however, current knowledge of the molecular mechanisms underlying the role of iron in neuronal function has remained scarce. In this work, we report novel findings

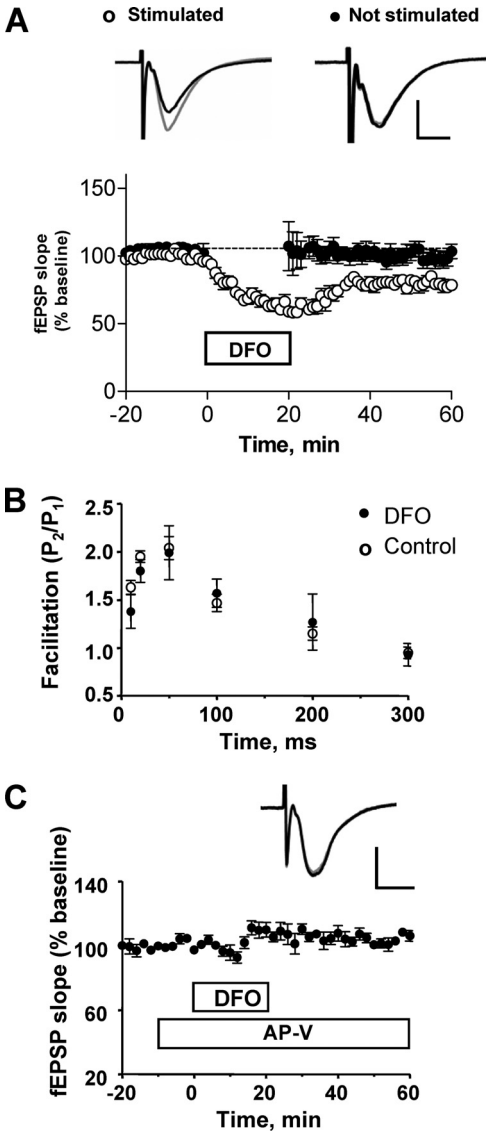

FIGURE 6. **Iron chelation with DFO induces a lasting depression of the CA1 synaptic responses to CA3 stimulation through a process requiring NMDA receptor activity.** *A*, effects of DFO addition to the bath for 20 min on a paired-pulse stimulation evoked (*fEPSP*) slope, registered in the CA1 area. Slices were electrically stimulated in the presence of 1 mM DFO (*open circles*). Alternatively, stimulation was suspended during incubation with DFO (*filled circles*). In the absence of stimulation, DFO did not modify basal synaptic transmission. Representative fEPSP traces of the response to the first pulse were recorded immediately before the incubation period with DFO (*gray traces*) or 30 min after washout of the drug (*black traces*). *Open circles*, 11 slices, 7 animals; *closed circles*, 7 slices, 7 animals. *B*, DFO did not affect paired pulse facilitation at different interstimulus intervals (10, 20, 50, 100, 200, and 300 ms). Data are given as mean ± S.E. (control, $n = 3$; DFO, $n = 4$). *C*, time course of the response to the first pulse (facilitation) in slices preincubated with the NMDA receptor antagonist DL-2-amino-5-phosphonopentanoic acid (*AP-V*) (100 μM) for 5 min before addition of DFO. The graph shows the effects of DFO on the first response. Statistical differences were analyzed by two-tailed unpaired Student's *t* test ($n = 3$). In *A* and *C*, the calibration *bars* indicate 0.5 mV and 5 ms.

indicating that ROS generated by iron are required for NMDA-induced and RyR-mediated ERK1/2 phosphorylation/nuclear translocation in primary hippocampal neurons. The electrophysiological studies presented here also indicate that iron is needed for basal synaptic transmission and sustained hippocampal CA1 LTP.

Contrasting with the scant knowledge on the role of iron in synaptic plasticity, a large amount of information supports a function for Ca^{2+} in this process. Stimulation of NMDA receptors by strong synaptic activity generates robust Ca^{2+} signals that stimulate the ERK1/2 cascade (40, 51) presumably via Ras activation (52). Nuclear translocation of the phosphorylated ERK1/2 proteins promotes the subsequent downstream phosphorylation of transcription factor CREB at serine 133, a requisite step for the CREB-dependent gene expression that underlies NMDA receptor-dependent late phase LTP at hippocampal CA3 to CA1 synapses (53).

Here, we found that stimulation of primary hippocampal cultures with NMDA elicited a sustained cellular Ca^{2+} concentration increase that was composed of an early and a late component. Ryanodine and the iron chelator DFO abolished the late component, an indication that both RyR and iron are needed for the sustained Ca^{2+} increase elicited by NMDA receptor stimulation. In addition, we show that ryanodine or iron chelation inhibited both NMDA-induced ERK1/2 phosphorylation and nuclear translocation of the phosphorylated ERK1/2 proteins, suggesting that functional RyR and iron are essential to generate the Ca^{2+} signals needed to fully stimulate the ERK pathway by NMDA.

Previous work by our group showed that iron stimulates RyR-mediated Ca^{2+} release in PC12 cells (28). In this work, we expanded those observations to hippocampal neurons in culture. We found that iron addition produced a fast LIP increase, suggesting that iron readily enters neuronal cells. The LIP increase was associated with ROS production, as determined by DCF fluorescence. We propose that iron stimulates RyR-mediated Ca^{2+} release through its capacity to generate ROS. Redox-active cations such as Fe^{2+} and Cu^{+} contribute to generate superoxide anion via the Haber-Weiss reaction (13). Superoxide rapidly dismutates to hydrogen peroxide, a mild oxidant that when added to primary hippocampal neurons produces redox modifications of the highly redox-sensitive RyR Ca^{2+} release channel, prompting the emergence of RyR-mediated Ca^{2+} signals that stimulate ERK and CREB phosphorylation (29).

Our previous studies with single RyR channels from muscle and brain have shown that the RyR redox state determines RyR activation by Ca^{2+}, so that only oxidized RyR are activated by increases in $[Ca^{2+}]$ within the physiological range (54, 55). Accordingly, we propose that hippocampal neurons require iron to provide the cellular ROS necessary to modify RyR, a requisite condition for their efficient activation via Ca^{2+}-induced Ca^{2+} release after NMDA receptor stimulation. This proposal provides an explanation for the inhibitory effects of DFO on the long-lasting NMDA-induced Ca^{2+} signals that promote ERK1/2 phosphorylation. Moreover, we show here that iron chelation with DFO abolished the RyR-dependent ERK1/2 phosphorylation increase produced by H_2O_2 in hippocampal slices. These results support our proposal that iron-mediated ROS generation is required to stimulate RyR-mediated Ca^{2+} release.

Synaptic plasticity is an activity-dependent neuronal response associated with learning and memory that entails significant modifications in the efficacy of synaptic transmission

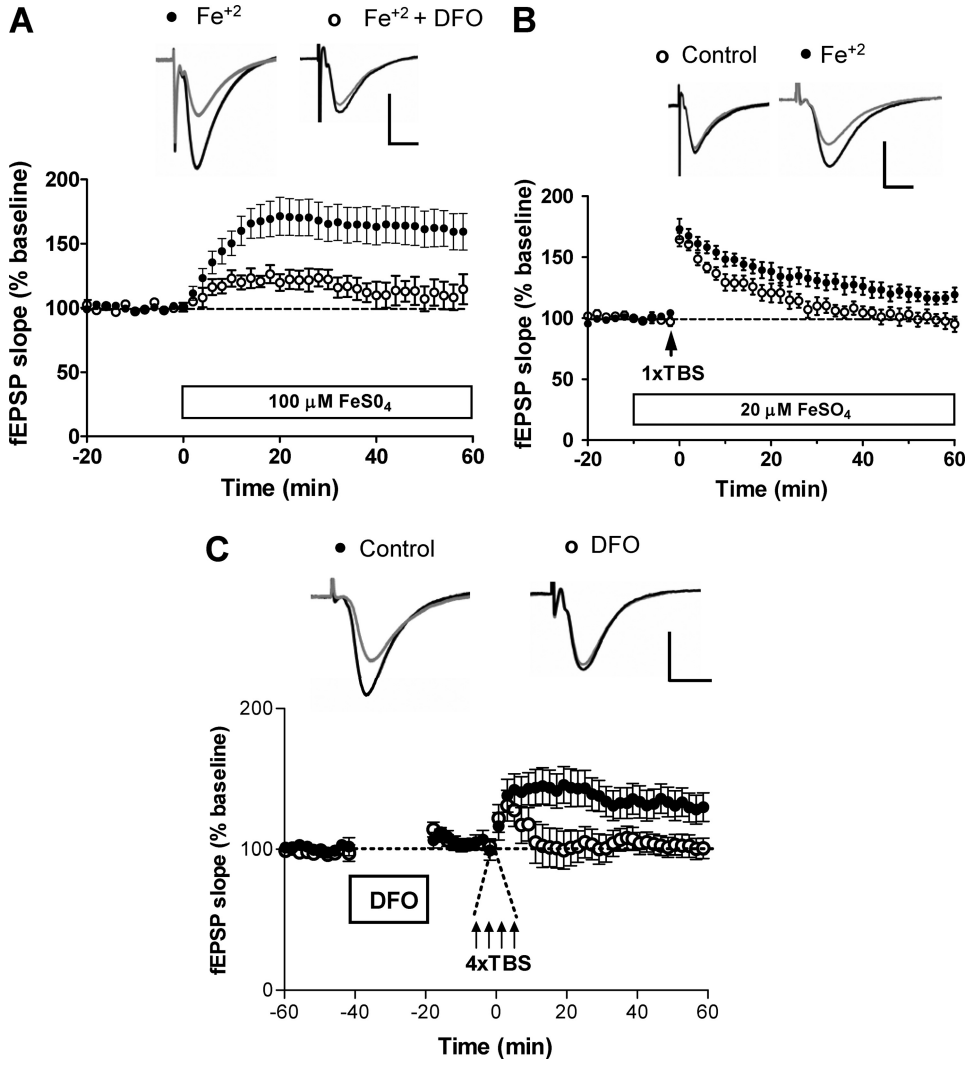

FIGURE 7. **Iron addition enhances synaptic transmission and LTP induction, whereas iron chelation with DFO inhibits LTP induction.** *A*, effects of bath application of 100 μM $FeSO_4$ (*open horizontal bar*) on paired-pulse stimulation-evoked fEPSP slopes in control slices (*solid circles,* 11 slices, 4 animals) or in slices preincubated for 1 h with 1 mM DFO (*open circles*, 4 slices, 3 animals). fEPSPs were recorded from the CA1 area; the representative traces shown were registered 10 (*gray traces*) or 60 min (*black traces*) after bath application of 100 μM $FeSO_4$. Values represent mean ± S.E. *B*, bath application of 20 μM $FeSO_4$ paired with one train of the theta burst stimulation (*arrow*, *1xTBS*) enhanced late-phase potentiation (60 min) of the field EPSP slope (*solid circles*). One train tetanus alone (*open circles*) induced lower transient potentiation that returned to basal values after 1 h. Values represent mean ± S.E. *Open circles*, 19 slices, 6 animals; *closed circles*, 14 slices, 6 animals. The representative traces shown were obtained 10 (*gray traces*) or 60 min (*black traces*) after the initial exposure to 100 μM $FeSO_4$ or ACSF. *C*, LTP was induced with four trains of tetanic theta burst stimulation (*arrows*) in control slices (*solid circles*; 19 slices, 6 animals) or in slices preincubated 40 min before stimulation with 1 mM DFO for 20 min (*open circles*, 14 slices, 6 animals). The representative traces shown were obtained 10 (*gray traces*) or 60 min (*black traces*) after stimulation. Data are given as mean ± S.E. Statistical differences were analyzed by two-tailed unpaired Student's *t* test. In all panels, the calibration *bar* indicates 0.5 mV and 5 ms.

(56–60). The role of Ca^{2+} release from intracellular stores in synaptic plasticity is broadly acknowledged (61). Functional RyR are required for hippocampal LTP, because RyR inhibition with dantrolene (27) or ryanodine (26) prevents long lasting CA1 hippocampal LTP induction. Calcium release is also important for both short-term and long-term plasticity in hippocampal glutamatergic synapses that are independent of NMDA receptor activity (62).

Only a few studies have addressed the role of iron on LTP (4, 6, 10). Pursuing this earlier work, we report here that iron chelation depressed basal synaptic transmission in hippocampal slices but did not affect paired pulse facilitation, suggesting a postsynaptic target for iron. The depression of basal synaptic transmission by DFO, an LTD-like response, required functional NMDA receptors because it was abrogated by the NMDA receptor inhibitor DL-2-amino-5-phosphonopentanoic acid. The requirement for functional NMDA receptors is an interesting observation that does not have an expeditious explanation. The postsynaptic Ca^{2+} signals generated in hippocampal CA1 dendritic spines during basal synaptic transmission are primarily derived from RyR-mediated Ca^{2+} release (63). We hypothesize that DFO, by decreasing significantly the postsynaptic $[Ca^{2+}]$ increase induced by NMDA in primary neurons, presumably reduces also the amplitude of Ca^{2+} signals in postsynaptic spines during basal synaptic transmission. The resulting low amplitude and short lasting postsynaptic Ca^{2+} signals generated in the presence of DFO, which are due solely to limited Ca^{2+} influx through NMDA receptors because DFO suppressed RyR-mediated Ca^{2+} release, may engage signaling cascades that inhibit AMPA receptor trafficking to the

postsynaptic membrane (64). Futures studies should address if this proposed mechanism accounts for the inhibition of basal synaptic transmission produced by iron chelation with DFO.

The present findings indicate that iron addition facilitated the induction of LTP with suboptimal tetanic stimulation, whereas iron chelation with DFO inhibited sustained LTP. Moreover, at higher concentrations iron produced an increased postsynaptic response even in the absence of stimulation, which was significantly prevented by preincubation with DFO. These combined results suggest that iron is needed post-synaptically to activate Ca^{2+}-dependent pathways downstream of NMDA receptors, including RyR-mediated Ca^{2+} release, which are required to maintain sustained hippocampal LTP.

We propose that the essential role of iron in LTP resides in its ability to stimulate the production of ROS needed to generate the robust postsynaptic Ca^{2+} signals required for ERK1/2 phosphorylation and the ensuing stimulation of downstream signaling cascades. Moreover, stimulation of NMDA receptors participates in neuronal iron homeostasis through activation of nitric oxide-dependent signaling cascades (25). Noteworthy, both NMDA and spatial memory training in a Morris water maze enhance the hippocampal expression of the iron transporter DMT1 (16), suggesting that neuronal activity stimulates this particular iron entry pathway to ensure an adequate iron supply.

In summary, the results presented here give strong support to a sequence of events whereby NMDA receptor stimulation leads to increased cytoplasmic [Ca^{2+}] and superoxide production, probably via NADPH oxidase (41). Superoxide dismutates to hydrogen peroxide, which reacts with iron to generate hydroxyl-free radicals. The resulting ROS increase would facilitate RyR-mediated Ca^{2+}-induced Ca^{2+} release via redox modification of the RyR protein. In turn, the ensuing intracellular [Ca^{2+}] increase would activate the ERK pathway as required for sustained LTP. Iron and RyR-mediated Ca^{2+} release play essential roles in this process, because their removal largely prevents ERK1/2 activation. These results highlight the central role of iron in neuronal processes, and may contribute to explain why iron deficiency is so deleterious to normal cognitive functions.

Acknowledgments—We thank Dr. Eric Klann for generous advice in the analysis of ERK1/2 phosphorylation in hippocampal slices, and Dr. Tatiana Adasme for help in composing the figures.

REFERENCES

1. Lozoff, B., Wolf, A. W., and Jimenez, E. (1996) *J. Pediatr.* **129,** 382–389
2. Lozoff, B., Jimenez, E., Hagen, J., Mollen, E., and Wolf, A. W. (2000) *Pediatrics* **105,** E51
3. Carlson, E. S., Stead, J. D., Neal, C. R., Petryk, A., and Georgieff, M. K. (2007) *Hippocampus* **17,** 679–691
4. McEchron, M. D., and Paronish, M. D. (2005) *Nutr. Neurosci.* **8,** 277–285
5. Ranade, S. C., Rose, A., Rao, M., Gallego, J., Gressens, P., and Mani, S. (2008) *Neuroscience* **152,** 859–866
6. Jorgenson, L. A., Sun, M., O'Connor, M., and Georgieff, M. K. (2005) *Hippocampus* **15,** 1094–1102
7. Maaroufi, K., Ammari, M., Jeljeli, M., Roy, V., Sakly, M., and Abdelmelek, H. (2009) *Physiol. Behav.* **96,** 343–349
8. Youdim, M. B. (2008) *Neurotox. Res.* **14,** 45–56
9. Carlson, E. S., Tkac, I., Magid, R., O'Connor, M. B., Andrews, N. C., Schallert, T., Gunshin, H., Georgieff, M. K., and Petryk, A. (2009) *J. Nutr.* **139,** 672–679
10. Hidalgo, C., and Núñez, M. T. (2007) *IUBMB Life* **59,** 280–285
11. Hidalgo, C., Carrasco, M. A., Muñoz, P., and Núñez, M. T. (2007) *Antioxid. Redox Signal.* **9,** 245–255
12. Pelizzoni, I., Macco, R., Zacchetti, D., Grohovaz, F., and Codazzi, F. (2008) *Biochem. Soc. Trans.* **36,** 1309–1312
13. Symons, M. C. R., and Gutteridge, J. M. C. (1998) *Free Radicals and Iron: Chemistry, Biology and Medicine*, Oxford University Press, New York
14. Gunshin, H., Mackenzie, B., Berger, U. V., Gunshin, Y., Romero, M. F., Boron, W. F., Nussberger, S., Gollan, J. L., and Hediger, M. A. (1997) *Nature* **388,** 482–488
15. Garrick, M. D., Singleton, S. T., Vargas, F., Kuo, H. C., Zhao, L., Knöpfel, M., Davidson, T., Costa, M., Paradkar, P., Roth, J. A., and Garrick, L. M. (2006) *Biol. Res.* **39,** 79–85
16. Haeger, P., Alvarez, A., Leal, N., Adasme, T., Nunez, M. T., and Hidalgo, C. (2009) *Neurotox. Res.* **17,** 238–247
17. Núñez, M. T., Gallardo, V., Muñoz, P., Tapia, V., Esparza, A., Salazar, J., and Speisky, H. (2004) *Free Radic. Biol. Med.* **37,** 953–960
18. Halliwell, B. (2006) *Plant Physiol.* **141,** 312–322
19. Halliwell, B. (2009) *Free Radic. Biol. Med.* **46,** 531–542
20. Kishida, K. T., and Klann, E. (2007) *Antioxid Redox. Signal.* **9,** 233–244
21. Bindokas, V. P., Jordán, J., Lee, C. C., and Miller, R. J. (1996) *J. Neurosci.* **16,** 1324–1336
22. Kahlert, S., Zündorf, G., and Reiser, G. (2005) *J. Neurosci. Res.* **79,** 262–271
23. Girouard, H., Wang, G., Gallo, E. F., Anrather, J., Zhou, P., Pickel, V. M., and Iadecola, C. (2009) *J. Neurosci.* **29,** 2545–2552
24. Brennan, A. M., Suh, S. W., Won, S. J., Narasimhan, P., Kauppinen, T. M., Lee, H., Edling, Y., Chan, P. H., and Swanson, R. A. (2009) *Nat. Neurosci.* **12,** 857–863
25. Cheah, J. H., Kim, S. F., Hester, L. D., Clancy, K. W., Patterson, S. E., 3rd, Papadopoulos, V., and Snyder, S. H. (2006) *Neuron* **51,** 431–440
26. Lu, Y. F., and Hawkins, R. D. (2002) *J. Neurophysiol.* **88,** 1270–1278
27. Obenaus, A., Mody, I., and Baimbridge, K. G. (1989) *Neurosci. Lett.* **98,** 172–178
28. Muñoz, P., Zavala, G., Castillo, K., Aguirre, P., Hidalgo, C., and Núñez, M. T. (2006) *Biol. Res.* **39,** 189–190
29. Kemmerling, U., Muñoz, P., Müller, M., Sánchez, G., Aylwin, M. L., Klann, E., Carrasco, M. A., and Hidalgo, C. (2007) *Cell Calcium* **41,** 491–502
30. Aguirre, P., Mena, N., Tapia, V., Arredondo, M., and Núñez, M. T. (2005) *BMC Neurosci.* **6,** 3
31. Epsztejn, S., Kakhlon, O., Glickstein, H., Breuer, W., and Cabantchik, I. (1997) *Anal. Biochem.* **248,** 31–40
32. Núñez-Millacura, C., Tapia, V., Muñoz, P., Maccioni, R. B., and Núñez, M. T. (2002) *J. Neurochem.* **82,** 240–248
33. Satoh, K., Ikeda, Y., Shioda, S., Tobe, T., and Yoshikawa, T. (2002) *Redox. Rep.* **7,** 219–222
34. Yamamoto, T., Yuki, S., Watanabe, T., Mitsuka, M., Saito, K. I., and Kogure, K. (1997) *Brain Res.* **762,** 240–242
35. Alford, S., Frenguelli, B. G., Schofield, J. G., and Collingridge, G. L. (1993) *J. Physiol.* **469,** 693–716
36. Bickel, H., Gaeumann, E., Keller-Schierlein, W., Prelog, V., Vischer, E., Wettstein, A., and Zaehner, H. (1960) *Experientia* **16,** 129–133
37. Keberle, H. (1964) *Ann. N.Y. Acad. Sci.* **119,** 758–768
38. Martell, A. E., and Smith, R. M. (1982) *Critical Stability Constants,* Vol. 5, Suppl. 1, p. 604, Plenum Press, New York
39. Neilands, J. B. (1995) *J. Biol. Chem.* **270,** 26723–26726
40. Krapivinsky, G., Krapivinsky, L., Manasian, Y., Ivanov, A., Tyzio, R., Pellegrino, C., Ben-Ari, Y., Clapham, D. E., and Medina, I. (2003) *Neuron* **40,** 775–784
41. Kishida, K. T., Pao, M., Holland, S. M., and Klann, E. (2005) *J. Neurochem.* **94,** 299–306
42. Sweatt, J. D. (2001) *J. Neurochem.* **76,** 1–10
43. Patterson, S. L., Pittenger, C., Morozov, A., Martin, K. C., Scanlin, H., Drake, C., and Kandel, E. R. (2001) *Neuron* **32,** 123–140
44. Núñez, M. T., Núñez-Millacura, C., Tapia, V., Muñoz, P., Mazariegos, D., Arredondo, M., Muñoz, P., Mura, C., and Maccioni, R. B. (2003) *Biometals* **16,** 83–90

45. Cadenas, E. (1989) *Annu. Rev. Biochem.* **58,** 79–110
46. Kruszewski, M. (2004) *Acta Biochim. Pol.* **51,** 471–480
47. Hidalgo, C., Donoso, P., and Carrasco, M. A. (2005) *IUBMB Life* **57,** 315–322
48. Marengo, J. J., Hidalgo, C., and Bull, R. (1998) *Biophys. J.* **74,** 1263–1277
49. Donoso, P., Aracena, P., and Hidalgo, C. (2000) *Biophys. J.* **79,** 279–286
50. Myhre, O., Andersen, J. M., Aarnes, H., and Fonnum, F. (2003) *Biochem. Pharmacol.* **65,** 1575–1582
51. Hetman, M., and Kharebava, G. (2006) *Curr. Top. Med. Chem.* **6,** 787–799
52. Cullen, P. J., and Lockyer, P. J. (2002) *Nat. Rev. Mol. Cell Biol.* **3,** 339–348
53. Thomas, G. M., and Huganir, R. L. (2004) *Nat. Rev. Neurosci.* **5,** 173–183
54. Bull, R., Finkelstein, J. P., Gálvez, J., Sánchez, G., Donoso, P., Behrens, M. I., and Hidalgo, C. (2008) *J. Neurosci.* **28,** 9463–9472
55. Bull, R., Finkelstein, J. P., Humeres, A., Behrens, M. I., and Hidalgo, C. (2007) *Am. J. Physiol. Cell Physiol.* **293,** C162–171
56. Gruart, A., Muñoz, M. D., and Delgado-García, J. M. (2006) *J. Neurosci.* **26,** 1077–1087
57. Bliss, T. V., and Collingridge, G. L. (1993) *Nature* **361,** 31–39
58. Bliss, T. V., and Lomo, T. (1973) *J. Physiol.* **232,** 331–356
59. Bailey, C. H., Kandel, E. R., and Si, K. (2004) *Neuron* **44,** 49–57
60. Fedulov, V., Rex, C. S., Simmons, D. A., Palmer, L., Gall, C. M., and Lynch, G. (2007) *J. Neurosci.* **27,** 8031–8039
61. Bardo, S., Cavazzini, M. G., and Emptage, N. (2006) *Trends Pharmacol. Sci.* **27,** 78–84
62. Lauri, S. E., Bortolotto, Z. A., Nistico, R., Bleakman, D., Ornstein, P. L., Lodge, D., Isaac, J. T., and Collingridge, G. L. (2003) *Neuron* **39,** 327–341
63. Emptage, N., Bliss, T. V., and Fine, A. (1999) *Neuron* **22,** 115–124
64. Hanley, J. G., and Henley, J. M. (2005) *EMBO J.* **24,** 3266–3278